Proceedings of the 2007 American Control Conference
Marriott Marquis Hotel at Times Square
New York City, USA, July 11-13, 2007

Enhanced Transparency in Haptics-Based Master-Slave Systems

M. Tavakoli, A. Aziminejad, R.V. Patel, M. Moallem
Department of Electrical & Computer Engineering, University of Western Ontario, London, ON, Canada N6A 5B9
Canadian Surgical Technologies & Advanced Robotics (CSTAR), 339 Windermere Road, London, ON, Canada N6A 5A5

Abstract— **Bilateral master-slave teleoperation, in addition to requiring a haptics-capable master interface, often requires one or more force sensors, which increases the cost and complexity of the system particularly for robot-assisted surgery. In this paper, we investigate the benefits of using force sensors that measure hand/master and slave/environment interactions, and study the effects of the bilateral control structure and in particular the presence of force feedforward and local force feedback on teleoperation transparency. Human factors experiments are performed to study how haptic feedback can help improve task performance under degraded visual conditions.**

I. Introduction

In master-slave teleoperation applications that deal with a delicate and sensitive environment such as soft-tissue surgery, it is important to provide feedback of slave/environment contact forces (haptic feedback) to the user's hand [1], [2]. Such a safety concern is especially significant if visual feedback to the surgeon is degraded, e.g., if fluids from the patient's body cloud the camera lens or the instruments leave the limited field of view of the endoscopic camera.

For feedback of instrument/tissue interactions to the surgeon's hand during master-slave surgery, the minimum requirement is to have a force-reflective human-machine interface, in which case it is possible to reflect forces to the user's hand merely based on the difference between the master and the slave positions and without actually measuring the forces resulting from instrument's contact with tissue. However, there are more advanced methods for haptic teleoperation control than such a "position error based" method. In fact, the presence of a force sensor on the slave robot for measuring the instrument/tissue interaction can lead to a more reliable haptic feedback.

The first question that we address in this paper is, regardless of the state of the technology in terms of meeting the requirements of haptic feedback in surgical robotic systems, what can haptic feedback deliver at its best during teleoperation on soft tissue? Toward this end, in Section II, we investigate the effect of force sensors on the slave side for measuring instrument/tissue interaction and on the master side for measuring hand/master interaction on the reliability of haptic feedback to the user. We also examine the effects of bilateral control structure and in particular the presence of force feedforward and local force feedback on teleoperation transparency.

This research was supported by the Natural Sciences and Engineering Research Council (NSERC) of Canada under grants RGPIN-1345 and RGPIN-227612, the Ontario Research and Development Challenge Fund under grant 00-May-0709 and infrastructure grants from the Canada Foundation for Innovation awarded to the London Health Sciences Centre (CSTAR) and the University of Western Ontario.

The second question in this paper is the following. The currently available surgical systems provide visual feedback but no haptic feedback to the surgeon, yet surgeons have relied on the visual feedback for performing complicated interventions such as coronary artery bypass grafting [3]. Can haptic feedback offer any help specially if the visual feedback is of poor quality? To answer this question, user performance is studied for a teleoperated soft tissue stiffness discrimination task when the visual feedback is corrupted but there is haptic feedback.

II. Transparent Haptic Teleoperation

Denoting the hand/master interaction as f_h and the slave/environment interaction as f_e, the dynamics of the master and the slave can be written as $f_m + f_h = M_m\ddot{x}_m$ and $f_s - f_e = M_s\ddot{x}_s$, where M_m, M_s, x_m, x_s, f_m and f_s are the master and the slave inertias, positions and control signals (force or torque), respectively. Transparency of a bilaterally controlled teleoperator depends on how well the slave-environment interaction forces are reflected to the users hand by the master [4]. To evaluate the transparency of teleoperation, the hybrid representation of the two-port network model of a master-slave system is most suitable:

$$\begin{bmatrix} F_h \\ -\dot{X}_s \end{bmatrix} = \begin{bmatrix} h_{11} & h_{12} \\ h_{21} & h_{22} \end{bmatrix} \cdot \begin{bmatrix} \dot{X}_m \\ F_e \end{bmatrix} \quad (1)$$

Note that velocities are used in the hybrid representation rather than positions, however stability and transparency are not affected by this convention. Perfect transparency is achieved if and only if the hybrid matrix has the following form

$$H_{\text{ideal}} = \begin{bmatrix} 0 & 1 \\ -1 & 0 \end{bmatrix} \quad (2)$$

For achieving the ideal response (2), various teleoperation control architectures are proposed in the literature. These control architectures usually classified as position-force (i.e. position control at the master side and force control at the slave side), force-position, position-position, and force-force architectures. Among these four architectures, in order to have a stiff slave, we are interested in the two cases in which the slave is under position control, namely position-position and force-position. A more general classification is by the number of communication channels required for transmitting position and force values from the master to the slave and vice versa in each bilateral control architecture. In the following, we introduce the commonly used position-position

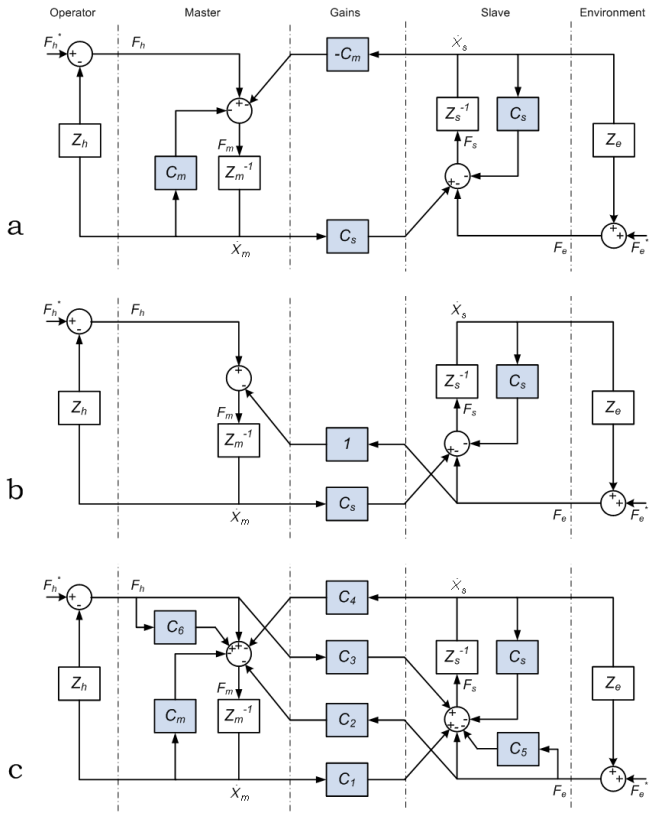

Fig. 1. (a) Position-error based, (b) direct force reflection, and (c) 4-channel bilateral control architectures. The shaded blocks represent control components.

and force-position two-channel architectures in addition to a more sophisticated four-channel architecture. We distinguish these architectures by the number of force sensors, if any, that are required in the system and compare their performances.

A. 2-channel (2CH) architectures

1) Position Error Based (PEB): A position-error based, also called position-position, teleoperation architecture is shown in Figure 1a. The impedances $Z_m(s) = M_m s$ and $Z_s(s) = M_s s$ represent the dynamic characteristics of the master robot and the slave robot, respectively. Also, $C_m = (k_{v_m} s + k_{p_m})/s$ and $C_s = (k_{v_s} s + k_{p_s})/s$ are proportional-derivative controllers used at the master and the slave, respectively (here the master and the slave velocities are fed to the two controllers).

As can be seen in Figure 1a, the PEB controller does not use any force sensor measurements (no shaded block with a force input) and merely tries to minimize the difference between the master and the slave positions, thus reflecting a force proportional to this difference to the user once the slave makes contact with an object. The hybrid matrix for this architecture is given as

$$H = \begin{bmatrix} Z_m + C_m \frac{Z_s}{Z_{ts}} & \frac{C_m}{Z_{ts}} \\ -\frac{C_s}{Z_{ts}} & \frac{1}{Z_{ts}} \end{bmatrix} \tag{3}$$

where $Z_{tm} = Z_m + C_m, \quad Z_{ts} = Z_s + C_s$. As a result, in addition to non-ideal force tracking ($h_{12} \neq 1$), the PEB method suffers from a distorted perception in free-motion condition ($h_{11} \neq 0$). This means that in the absence of a slave-side force sensor, control inaccuracies (i.e., nonzero position errors) lead to proportional force feedback to the user even when the slave is not in contact with the environment. To investigate the absolute stability of this system, assuming Z_h and Z_e are passive, we use Llewellyn theorem:[5]:

Theorem 2.1: The teleoperation system (1) is absolutely stable if and only if: (a) $h_{11}(s)$ and $h_{22}(s)$ have no poles in the right half plane (RHP); (b) any poles of h_{11}(s) and $h_{22}(s)$ on the imaginary axis are simple with real and positive residues; and (c) for $s = j\omega$ and all real values of ω

$$\Re(h_{11}) \geq 0 \tag{4}$$

$$\Re(h_{22}) \geq 0 \tag{5}$$

$$2\Re(h_{11})\Re(h_{22}) - \Re(h_{12}h_{21}) - |h_{12}h_{21}| \geq 0 \tag{6}$$

where $\Re(\cdot)$ and $|\cdot|$ denote the real and absolute values.

The characteristic polynomial for h_{11} and h_{22} is $M_s s^2 + k_{v_s} s + k_{p_s}$, which has no RHP poles if $k_{v_s}, k_{p_s} > 0$. With respect to conditions (4) and (5), we have

$$\Re(h_{11}) = \frac{M_s(k_{v_s}k_{p_m} - k_{v_m}k_{p_s} + M_s k_{v_m}\omega^2)}{k_{v_s}^2 + (-k_{p_s}/\omega + M_s\omega)^2} \tag{7}$$

$$\Re(h_{22}) = \frac{k_{v_s}}{k_{v_s}^2 + (-k_{p_s}/\omega + M_s\omega)^2} \tag{8}$$

which are non-negative if $k_{v_m} > 0$ and

$$k_{v_s}k_{p_m} - k_{v_m}k_{p_s} = 0 \tag{9}$$

Also, the equality to zero in condition (6) holds if (9) holds and $k_{v_m}, k_{p_m} > 0$.

2) Direct Force Reflection (DFR): A direct force reflection, also called force-position, teleoperation architecture is shown in Figure 1b. This method requires a force sensor to measure the interactions between the slave and the environment. The hybrid parameters for the force-position architecture are given as

$$H = \begin{bmatrix} Z_m & 1 \\ -\frac{C_s}{Z_{ts}} & \frac{1}{Z_{ts}} \end{bmatrix} \tag{10}$$

Consequently, while the perception of free-motion is still less than ideal ($h_{11} \neq 0$), perfect force tracking is attained ($h_{12} = 1$). Nonetheless, compared to the PEB method, h_{11} is much closer to zero in the DFR method and the user only feels the inertia of the master interface when the slave is not in contact. While the DFR method proves to be better than the PEB method, both methods suffer from the less-than-ideal h_{21} and h_{22} values, resulting in poor position tracking response and slave stiffness. In Section II-B, we will explain how a 4-channel architecture can fulfil all of the conditions of the ideal response (2).

To analyze the stability via Theorem 2.1, h_{11} has no poles and the characteristic polynomial for h_{22} is $M_s s^2 + k_{v_s} s + k_{p_s}$, which has no RHP poles if $k_{v_s}, k_{p_s} > 0$. Also, $\Re(h_{11}) = 0$ and $\Re(h_{22})$ is same as (8), which is non-negative if $k_{v_s} >$

0. Also, condition (6) is simplified to

$$\Re\left(\frac{C_s}{C_s+Z_s}\right)-\left|\frac{C_s}{C_s+Z_s}\right|\geq 0 \qquad (11)$$

Equation (11) holds if and only if

$$\Im\left(\frac{C_s}{C_s+Z_s}\right)=\frac{k_{v_s}\omega M_s}{k_{v_s}^2+(-k_{p_s}/\omega+M_s\omega)^2}=0 \qquad (12)$$

which is mathematically true provided $k_{v_s}=0$, i.e., no derivative term is used at the slave side, which is not a viable option. However, the imaginary part (12) approaches zero if $k_{p_s}\to\infty$, $k_{v_s}\to\infty$ or $M_s\to 0$, which can all be summarized as $|C_s|\gg|Z_s|$. Finally, using a low-pass filter can help to achieve a higher degree of absolute stability.

The above discussion is conservative as it ensures stability regardless of the teleoperation system's terminations. For a less conservative study, taking into account the remote environment impedance Z_e, i.e., $F_e=Z_e\dot{X}_s$, the general teleoperation system given by (1) has the following transfer function from F_h to $\dot{X}_m$:

$$\frac{\dot{X}_m}{F_h}=\frac{1+h_{22}Z_e}{h_{11}(1+h_{22}Z_e)-h_{12}h_{21}Z_e} \qquad (13)$$

Assuming the environment is modeled by a linear spring, $Z_e=k_e/s$, the characteristic equation for the transfer function from F_h to $\dot{X}_m$ (and to any other output), which must have no zeros in the right-half plane (RHP) for the teleoperation system to be stable, is given by

$$h_{11}s+k_e(h_{11}h_{22}-h_{12}h_{21})=0 \qquad (14)$$

Using the hybrid parameters (10) and $C_s=(k_{v_s}s+k_{p_s})/s$, (14) simplifies to

$$M_mM_ss^4+M_mk_{v_s}s^3+M_m(k_e+k_{p_s})s^2+k_ek_{v_s}s+k_ek_{p_s}=0 \qquad (15)$$

Applying the Routh-Hurwitz theorem to (15), the necessary and sufficient conditions for asymptotic stability of the teleoperation system are

$$\Delta_1=\frac{k_{v_s}}{M_s}>0,\quad \Delta_2=\frac{k_{v_s}[\beta k_{p_s}+k_e(\beta-1)]}{M_sM_m}>0$$
$$\Delta_3=\frac{k_{v_s}^2k_e^2(\beta-1)}{M_s^2M_m^2}>0,\quad \Delta_4=\frac{k_{v_s}^2k_e^3k_{p_s}(\beta-1)}{M_s^3M_m^3}>0 \qquad (16)$$

where $\beta=M_m/M_s$. The above condition set holds iff

$$k_{v_s}>0,\quad k_{p_s}>0,\quad \beta>1 \qquad (17)$$

While we have considered a unity force feedback gain in Figure 1b, if a gain $k_f\neq 1$ is used, the condition $\beta>1$ is changed to $\beta>k_f$. The condition set (17) guarantees stability independent of frequency. In practice, however, the limited bandwidth of physical systems and additional low-pass filtering help relax the above requirements so that the system is stable even for $\beta<1$.

B. 4-channel (4CH) architecture

Figure 1c depicts a general 4-channel (4CH) bilateral teleoperation architecture [4], [6]. This architecture can represent all teleoperation structures through appropriate selection of subsystem dynamics C_1 to C_6. The local force feedback compensators C_5 and C_6 shown in Figure 1c improve stability and performance of the system. In contrast to 2CH architectures, a sufficient number of parameters (degrees of freedom) in the 4CH architecture enables it to achieve ideal transparency. In fact, by selecting C_1 through C_6 according to

$$C_1=Z_{ts},\quad C_2=1+C_6,\quad C_3=1+C_5,\quad C_4=-Z_{tm} \qquad (18)$$

the ideal transparency conditions (2) are fully met [7].

1) 3-channel (3CH) case: Another potential benefit of the general 4CH architecture of Figure 1c is that by proper adjustment of the local feedback parameters, it is possible to obtain two classes of 3CH control architectures, which can be transparent under ideal conditions [7], [8]. The first class of 3CH architectures is derived by setting $C_2=1$ and $C_3=0$. As a consequence, $C_5=-1$ and $C_6=0$. In other words, there is no need for master/operator interaction force measurement and therefore, the number of the sensors in the system can be reduced. The second class of 3CH architectures is obtained by setting $C_2=0$ and $C_3=1$. In this class, force measurement at the slave side is not needed. The need for fewer sensors without imposing additional expense on system transparency makes the 3CH architectures extremely attractive from the implementation point of view.

III. Haptic Teleoperation Experiments

A. Experimental setup

For experimental evaluation of different haptic teleoperation control methods, we have used a 1-DOF bilateral master-slave system developed for endoscopic surgery experiments [8]. The master and the slave effective inertias were identified to be $M_m=5.968\times10^{-4}$ kgm^2 and $M_s=9.814\times10^{-3}$ kgm^2, respectively.

B. Soft-tissue palpation tests

In a palpation test, the user twists the master back and forth causing the slave to repeatedly probe a soft tissue using a small rigid beam attached to the slave's end-effector for 60 seconds.

Figure 2 shows the master and the slave position and torque tracking profiles for the PEB teleoperation system. Figure 3 illustrates the same profiles for the DFR system. As can be seen, the position tracking performance is satisfactory for both of these systems. However, the DFR system displays a superior force tracking performance compared to PEB.

Next, a second set of free-motion tests is performed, which in conjunction with the previous contact-mode tests, can be used to determine the hybrid parameters of the teleoperation system in the frequency domain according to the method described in [8]. The magnitudes of the hybrid parameters of the PEB and DFR teleoperation systems are shown in Figure 4. Figure 4 is an indication of DFR's superiority in terms of transparent performance considering the ideal transparency requirements outlined by (2). Relatively high

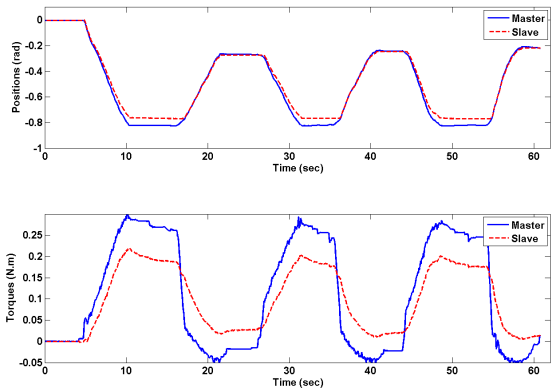

Fig. 2. Position and force profiles for the PEB teleoperation system.

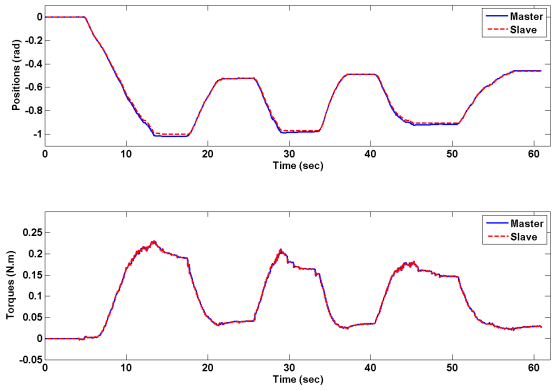

Fig. 3. Position and force profiles for the DFR teleoperation system.

values of h_{11} for PEB are evidence of the fact that even when the slave is in free space, the user will feel some force, giving a "sticky" feel of free-motion movements. On the other hand, since DFR uses f_e measurements, its input impedance in free-motion condition (h_{11}) will be lower making the feeling of free space much more realistic. The better force tracking performance of DFR, i.e., $h_{12} \approx 0$ dB, confirms the time-domain plots of Figures 2 and 3. With regard to h_{21}, both spectra are close to 0 dB, which indicates both systems ensure good position tracking. These results are in accordance with equations (3) and (10). It is worthwhile mentioning that because of the finite stiffness of the slave and also the backlash present in the slave's gearhead, the accuracy of $h_{22} = -X_s/F_e|_{X_m=0}$ estimates is less than that of the rest of the hybrid parameters.

Figure 5 shows the master and the slave position and torque tracking profiles for the 3CH teleoperation system in which $C_2 = 1$, $C_6 = 0$, $C_3 = 0$ and $C_5 = -1$. Figures 6 and 7 show similar profiles for the same choice of C_2 and C_6 but for $C_3 = 0.5$, $C_5 = -0.5$ and $C_3 = 1$, $C_5 = 0$, respectively. As can be seen, as the local force feedback gain at the slave is reduced (i.e., lower $|C_5|$), the (steady-state) force tracking performance deteriorates. The superiority of performance in the case of the 3CH architecture can be attributed to the higher gain of the slave local feedback, which allows for lower level of master force feedforward (i.e., lower C_3) and consequently less contribution from the hand force observer. The magnitudes of the hybrid parameters of the

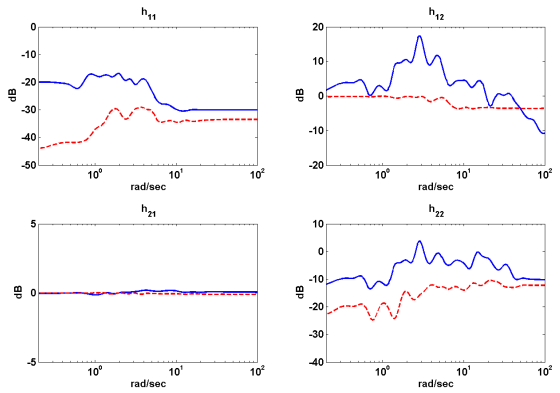

Fig. 4. Magnitudes of the hybrid parameters for 2CH architectures (solid: PEB, dashed: DFR)

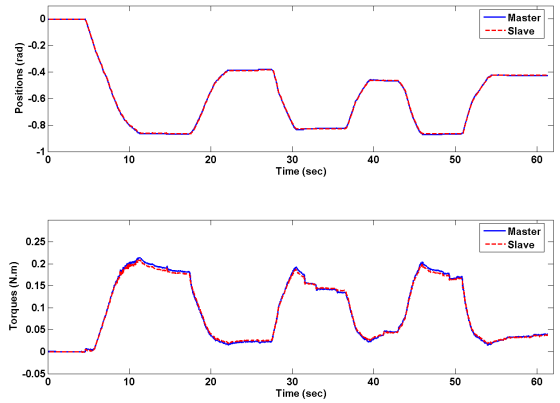

Fig. 5. Position and force profiles for the 3CH architecture with $C_3 = 0$ and $C_5 = -1$.

3CH and the two 4CH teleoperation systems are shown in Figure 8. As it can be seen, the magnitude of h_{12} over low frequencies, which is indicative of steady-state force tracking error, increases above 0 dB as the gain of slave local force feedback is reduced.

Although based on Figures 3 and 5 it seems that the DFR architecture can offer a performance comparable to the 3CH architecture, it must be noted that the above experiments have been performed using a soft object (a silicon-based tissue phantom placed on top of a layer of packaging foam). Under hard contact (using a piece of wood instead of the tissue phantom), however, the DFR shows less than satisfactory position tracking (Figure 9) while the 3CH performs satisfactorily in terms of both position tracking (Figure 9) and force tracking (not shown).

IV. The Effect of Haptic Feedback Under Degraded Visual Conditions

Video streaming over IP networks is increasingly becoming the technology of choice for a wide range of network multimedia applications including live video transmission in telerobotics-assisted surgery and therapy. In this method of transmission, the video quality can be easily affected by network congestion resulting in poor video quality at the surgeon side [9]. In the absence of haptic sensation for the surgeon, degraded visual conditions can make it difficult to prevent tissue damage. In this section, our goal is to study

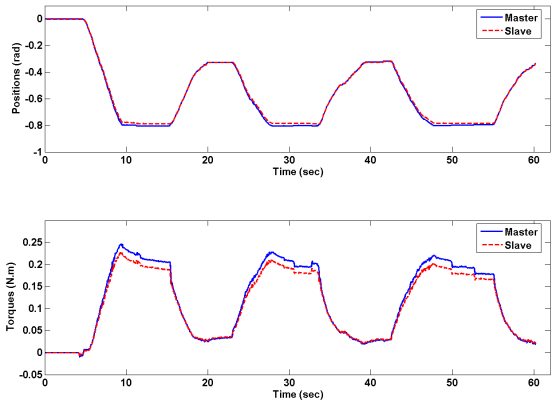

Fig. 6. Position and force profiles for the 4CH architectures with $C_3 = 0.5$ and $C_5 = -0.5$ (4CH-1).

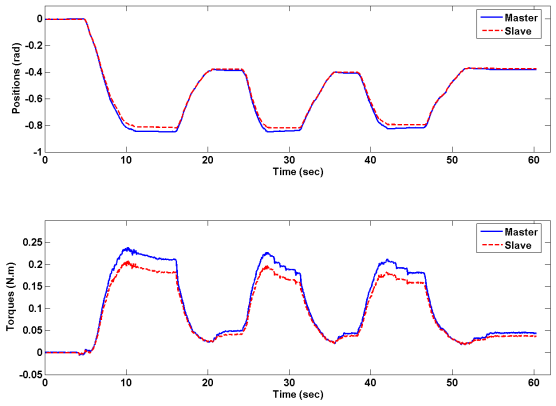

Fig. 7. Position and force profiles for the 4CH architectures with $C_3 = 1$ and $C_5 = 0$ (4CH-2).

how effectively haptic cues can replace a corrupted visual feedback during a soft-tissue stiffness discrimination task.

A. Experiment Design

Using the master-slave system, teleoperation experiments were conducted in which the task is to discriminate between any two soft tissues with different stiffnesses through telerobotic palpation. "Tissue palpation" is one of the ways to detect cancerous tissue which has a different stiffness compared to healthy tissue. Visual and haptic feedback modalities are compared in terms of their capability in transmitting critical task-related information to the user. In our experimental scenario, the visual link consisted of a 320×240 webcam-provided image, which is transmitted from the slave side to the master side via a H.323-based NetMeeting Internet video-conferencing application at a rate of 14 frames per second. The communication media was a 1000T-base Ethernet network. Due to its satisfactory performance, the 3CH architecture described in this paper was used for bilateral teleoperation control.

Six subjects (3 males and 3 females) aged 24-34 participated in our experiments. The subjects had average exposure to haptic cues and average experience with the master-slave system. The subjects' primary goal was defined as distinguishing between different tissues in terms of their relative stiffness.

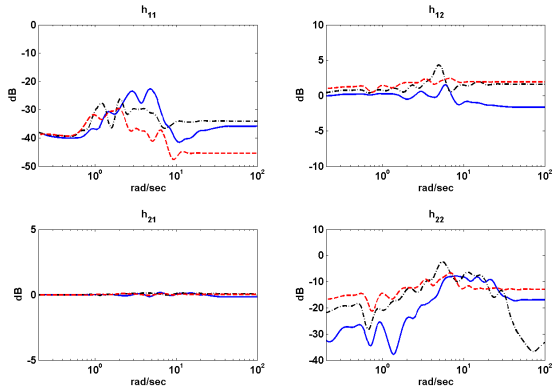

Fig. 8. Magnitudes of the hybrid parameters for 4CH architectures (solid: 3CH, dash-dot: 4CH-1, dashed: 4CH-2).

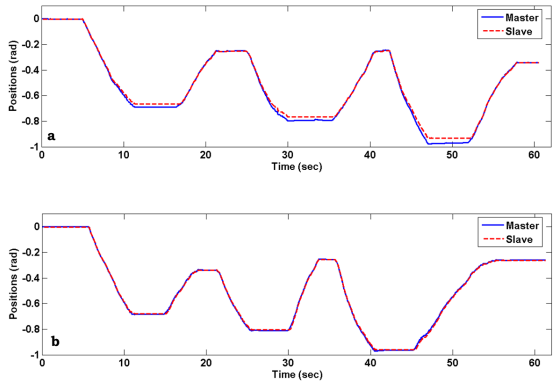

Fig. 9. Position profiles for (a) DFR and (b) 3CH architectures under hard contact.

In each trial, one out of the two feedback modalities and a combination of two out of three different tissue samples (two different tissues or the same tissue twice) were presented to the subject. Since our intention was to study the utility of haptic feedback under degraded or suppressed visual conditions, camera vision from the slave side was switched off when the subjects received haptic feedback so that visual cues did not play a role. In total, each subject made 8 trials (i.e., 8 randomly selected combinations of feedback modality and tissue pair). The trials were presented in a randomized order to the subjects.

In each trial, the tool/tissue interaction forces, the end-effector position, and the task completion time were recorded. In addition to task success rate and task times, we also compared the energy supplied to tissue since lower energy corresponds to less trauma and probably less tissue damage. The energy was calculated as $\int_0^T f(t)v(t)\mathrm{d}t$ where T, f, and v are the task completion time, contact force, and slave's velocity, respectively.

B. Results

The test results for the palpation task are shown in Figure 10 in the form of bar graphs of mean values. Figure 10a shows the task success rates for the two different feedback modes. Due to the pass/fail nature of the tests (1: successful; 0: unsuccessful) and for an accurate analysis, we used a two-tailed t-test between the two feedback modes, which

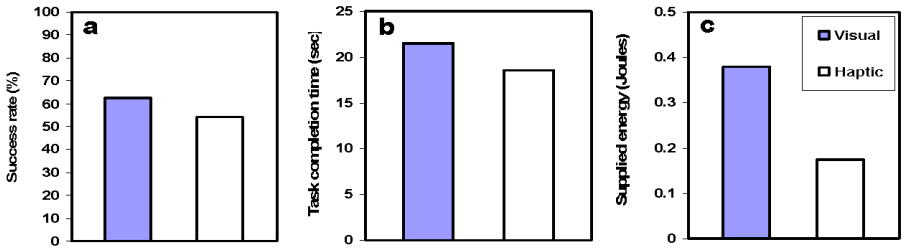

Fig. 10. (a) Mean success rate; (b) mean completion time (sec); (c) mean energy supplied to the tissue (Joul) for a soft tissue stiffness discrimination task.

indicates that the success rates for visual and haptic modes are not significantly different ($t(24) = 2.069$, $p = 0.538$).

The bar graph of Figure 10b represents the mean values of task completion times (seconds) for the two feedback modes. A two-tailed t-test ($t(24) = 2.069$, $p = 0.0285$) confirms that the task completion times are longer under visual feedback than haptic feedback.

Figure 10c shows the mean values of the energy supplied to tissue (Joules). A two-tailed t-test ($t(24) = 2.069$, $p = 0.0037$) confirms that the mean supplied energy for the visual mode is significantly higher than that for the haptic mode.

C. Discussion

After analyzing the results of the palpation trials, the following trends were observed:

Since a subject had to decide whether the two tissue samples were "similar", "the first one softer compared to the second one", and "the first one harder compared to the second one", the chance level was 33%. Therefore, both of the success rates are well above this chance level. The close success rates show that for a task involving the comparison of force/deformation tissue characteristics, haptic feedback can effectively replace a corrupted visual cue.

As for the success rate with visual cues, it was observed during the experiments that the depth of tissue indentation could not be precisely quantified by the subjects. The success rate for visual cues strongly depends on the video's information content, which in turn can be attributed to various task-dependent and task-independent factors ranging from network conditions for IP-based video streaming to the camera's angle of view. For example, task performance might be seriously degraded if critical movements of the task are orthogonal to the camera view causing depth perception problems.

With respect to task completion time, one's expectation would be that haptic cues result in considerably shorter task times, but in practice the tissue stiffnesses were not significantly different and subjects needed to palpate each tissue usually more than once. In terms of supplying energy and consequently incurring damage/injury to tissue, the visual mode resulted in poor performance. The reason is that a subject had to supply a significant amount of energy before tissue deformations were quantifiable. The haptic mode is clearly better as it results in a noticeably less supply of energy to tissue.

V. Concluding Remarks

This paper studied the stability and transparency of 2-channel and 4-channel bilateral teleoperation control architectures. Using a haptics-capable master-slave test-bed to study the effect of including force sensor measurements in teleoperation control, it was found that slave/environment force measurement can significantly improve teleoperation transparency in a 2-channel architecture. In contrast to 2-channel architectures, a sufficient number of design parameters in the 4-channel architecture enables it to achieve ideal transparency. If a 3-channel bilateral control is used, slave local force feedback can eliminate the need for hand/master force measurements at no penalty on transparency. We also compared users performance under visual and haptic modalities for a soft-tissue stiffness discrimination task. The goal was to study how effectively haptic cues can replace a corrupted visual cue. It was found that haptic cueing leads to an equal rate of success in discriminating between two tissue samples with different stiffnesses, while visual cueing incurs the highest risk of tissue damage due to excessive tissue deformation.

References

[1] C. Wagner, N. Stylopoulos, and R. Howe, "The role of force feedback in surgery: Analysis of blunt dissection," in *10th Symp. on Haptic Interfaces for Virtual Environment and Teleoperator Systems*, Orlando, 2002, pp. 68–74.

[2] G. T. G, J. P. Desai, and A. E. Castellanos, "Force feedback plays a significant role in minimally invasive surgery: results and analysis," *Annals of Surgery*, vol. 241, no. 1, pp. 102–109, 2005.

[3] E. J. Stephenson, S. Sankholkar, C. T. Ducko, and R. J. J. Damiano, "Robotically assisted microsurgery for endoscopic coronary artery bypass grafting," *The Annals of Thoracic Surgery*, vol. 66, no. 3, pp. 1064–1067, 1998.

[4] D. A. Lawrence, "Stability and transparency in bilateral teleoperation," *IEEE Transactions on Robotics & Automation*, vol. 9, pp. 624–637, October 1993.

[5] S. Haykin, *Active Network Theory*. Reading, MA: Addison-Wesley, 1970.

[6] Y. Yokokohji and T. Yoshikawa, "Bilateral control of master-slave manipulators for ideal kinesthetic coupling–formulation and experiment," *IEEE Transactions on Robotics and Automation*, vol. 10, no. 5, pp. 605–620, 1994.

[7] K. H. Zaad and S. E. Salcudean, "Transparency in time delay systems and the effect of local force feedback for transparent teleoperation," *IEEE Transactions on Robotics and Automation*, vol. 18, no. 1, pp. 108–114, 2002.

[8] M. Tavakoli, R. V. Patel, and M. Moallem, "Bilateral control of a teleoperator for soft tissue palpation: design and experiments," *IEEE International Conference on Robotics and Automation*, pp. 3280–3285, 2006.

[9] D. Wu, Y. T. Hou, W. Zhu, Y. Q. Zhang, and J. M. Peha, "Streaming video over internet: approaches and directions," *IEEE Transactions on Circuits and Systems for Video Technology*, vol. 11, pp. 282–300, 2001.